

G. van der Schrier · S.L. Weber · S.S. Drijfhout

## Sea level changes in the North Atlantic by solar forcing and internal variability

Received: 17 August 2001 / Accepted: 18 February 2002 / Published online: 15 May 2002  
© Springer-Verlag 2002

**Abstract** Sea level change due to variations in the thermohaline structure of the North Atlantic has been calculated using a coupled ocean–atmosphere model of intermediate complexity (ECBilt). Two 1000-year simulations are made, one using a constant solar forcing and one using an estimate of historic variations in solar activity. In the solar forced simulation sea level variations are a proxy for climate variations. Anomalies in sea surface temperature (SST) of the northern North Atlantic are generated by the solar radiation changes. These SST anomalies modulate the ocean thermohaline circulation (THC), affecting surface salinities in the northern North Atlantic which are subsequently advected to the deep ocean. The associated deep ocean geopotential thickness anomalies dominate sea level in the North Atlantic and are advected southwards with the overturning circulation. Sea level change in the solar forced simulation is primarily an indirect response to solar radiation changes, which modulate the THC. In the unforced run, changes in the THC affect sea level in a similar way. However, in this simulation THC variability is no longer generated by sea surface temperature variations but by sea surface salinity variations, resulting from internal climate dynamics. The present results will aid in analyses of reconstructed low-frequency sea-level variations based on proxy data.

level and geopotential thickness (Levitus 1990). Numerical modelling has related these changes in the hydrography to changes in the strength of the Gulf Stream/North Atlantic Drift (Greatbatch et al. 1991, 1996; Häkkinen 1999). These and other (Ezer 2001; Häkkinen 2001) results indicate that observed sea level at the US east coast may act as proxy for overturning circulation variations on interannual to decadal time scales, provided that the effects of baroclinic Rossby waves on coastal sea level are subtracted. Existing model studies relating sea level to the overturning cover just a few decades and instrumental records for sea level typically span some 100 years. Recent reconstructions of sea level at the US east coast based on foraminiferal analysis span some 1500 years (van de Plassche 2000, van de Plassche et al. 1998). These reconstructions show rapid and frequent variations on decadal and centennial time scales; the latter time scale is an order of magnitude larger than thus far considered by existing sea level model studies. The question whether sea level variations on centennial time scales can be related to overturning in a similar way as on decadal time scales, remains to be settled.

Sea level variations can be brought about by variations in atmospheric pressure, or the ‘inverted barometer effect’, variations in windstress and changes in steric sea level. In areas with low atmospheric pressure the sea surface is higher and vice versa. Changes in windstress exerted on the ocean surface will change the Ekman transport, convergences or divergences will develop and the sea level pattern will change. The steric sea level is high when the water is warm, low when it is cold. Conversely, a high steric sea level corresponds to a low value of salinity. Mass changes of mountain glaciers and ice sheets are of importance for sea-level variations, but are excluded in this study.

Sources for changes in the hydrography of the North Atlantic include variations in the ocean–atmosphere buoyancy exchange or variations in the overturning circulation itself. Changes in the buoyancy forcing may be caused by internal variability of the coupled

---

### 1 Introduction

Substantial changes over recent decades in the thermohaline structure of the North Atlantic have been documented which gave rise to variations in its steric sea

---

G. van der Schrier (✉) · S.L. Weber · S.S. Drijfhout  
KNMI, PO Box 201, 3730 AE De Bilt,  
The Netherlands  
E-mail: schrier@knmi.nl

ocean–atmosphere system, or by external forcing like solar variability. A clear understanding of the Sun–climate relationship (including the oceanic climate) is hampered by the uncertainty of the mechanism relating solar activity to climate (Haigh 1996; Reid 1999). Nevertheless, a considerable amount of evidence exists for a significant impact of solar variability on climate, although most of these empirical studies focus on the effects on atmospheric variables (Lean and Rind 1998; van Loon and Labitzke 1998, 1999; van der Schrier and Versteegh 2001) or the upper ocean temperature (Barnett 1989; White et al. 1997). Changes in the radiative output of the Sun will certainly have a direct effect on the thermal structure of the oceanic upper layer, but an indirect response on oceanic climate by affecting the internal variability of the ocean is also possible.

The objective of this study is to explore the causes of low-frequency sea level variations in the North Atlantic, both for a free (constant forcing) simulation and a solar forced simulation. In this study we will show that variability in North Atlantic sea level on the decadal and centennial time scales is dominated by variations in its density stratification. The time scales and time span of interest here reflects the temporal resolution and length of the proxy records for sea level, which are typically decadal–centennial, and some thousand years respectively.

Earlier modelling studies which assessed the influence of long-term solar variability on climate include energy balance model (EBM) studies (Crowley 2000; Crowley and Kim 1999), general circulation models (GCMs) (Cubasch et al. 1997; Rind et al. 1999) and GCMs of intermediate complexity (Drijfhout et al. 1999). The ocean merely acts as a storage of heat in the EBMs. On the other hand, the (advanced and intermediate complexity) GCMs feature a dynamically active ocean (except that of Rind et al. 1999), but their analysis did not extend to the time span used in the EBM studies. The present work intends to combine these approaches, focusing on the impact of solar activity on sea level change.

We use a coupled atmosphere–ocean model of intermediate complexity (ECBilt) (Opsteegh et al. 1998). To assess the role of internal climatic variations, we analyze a 1000 year control run with ECBilt. In addition, we analyze a 1000 year run forced with a reconstruction from a proxy record of solar irradiance to assess the role of variations in solar activity in North Atlantic sea level. Changes in orbital parameters over the last 1000 years result in very small changes in irradiance and are not considered. The control run has previously been described and analyzed by Selten et al. (1999). Solar forced runs with ECBilt have previously been conducted with ECBilt (Drijfhout et al. 1999; Haarsma et al. 2000) using idealized rather than realistic irradiance variations. Other climate variability studies using ECBilt include Drijfhout et al. (2001), Goosse et al. (2000), Haarsma et al. (2001), Renssen et al. (2001) and Weber (2001).

This study is organized as follows: in Section 2 a short description of the model is presented and the computations of sea level variations is discussed in the light of various approximations in the dynamics and model formulation. Results from the control run and the solar forced run are presented in Sects. 3 and 4 respectively. Finally, Sect. 5 gives a discussion and conclusions.

## 2 Model description

The atmospheric component of ECBilt resolves 21 wavelengths around the globe. It contains 3 levels in the vertical. The dynamical part is an extended quasi-geostrophic model where the neglected ageostrophic terms are included in the vorticity and thermodynamic equations as a time dependent and spatially varying forcing. With this forcing the model simulates the Hadley circulation qualitatively correct, and the strength and position of the jet stream and transient eddy activity become fairly realistic in comparison to other T21 models. The essentials of baroclinic instability are included, but the variability associated with it is underestimated compared to observations. The model contains simple physical parametrizations, including a full hydrological cycle. The cloud coverage is prescribed to climatological values, an acceptable simplification since earlier modelling results (Rind et al. 1999) suggest that cloud cover variations are relatively independent of solar forcing changes. Moreover, if the cloud cover feedback is important, it is likely to be an amplifying feedback. Neglect of this feedback will not give a qualitative change of the model results. The atmospheric component is coupled to a simple, low resolution ( $\sim 5.6^\circ$ ) GFDL-type, flat-bottomed ocean model with 12 unevenly spaced levels in the vertical and a thermodynamic sea-ice model.

The ocean–atmosphere fluxes for heat, salt and momentum involve the two top layers of 30 m and 50 m respectively. The time step of the atmospheric model is 4 h, whereas the ocean model has a time step of 1 day.

The coupled model is realistic in the sense that it contains the minimal amount of physics that is necessary to simulate the mid-latitude planetary and synoptic scale circulations. It displays realistic internal climate oscillations on the decadal time scale (Selten et al. 1999). The patterns of variability have strong similarities with observed patterns, although the amplitude of variability is too small (Opsteegh et al. 1998). The coupled model operates without having to resort to flux adjustment.

The initial state used for both the free, unforced, simulation and the solar-forced simulation contained a slow drift in the temperature ( $0.6 \times 10^{-3} \text{ K year}^{-1}$ ) and salinity ( $-1.4 \times 10^{-4} \text{ psu year}^{-1}$ ) in the deep ocean (900–4000-m). The North Atlantic Ocean is too warm and too saline, but the main features of the different water masses are present, although too diffuse compared to measurements (Opsteegh et al. 1998). The anomalously high temperatures in the North Atlantic prevent the sea ice playing a significant role in the variability of the North Atlantic thermohaline structure or in the variability of North Atlantic Deep Water (NADW) formation. The amount of NADW formed in the model at high latitudes is about 12 Sv ( $1 \text{ Sv} = 10^6 \text{ m}^3 \text{ s}^{-1}$ ), somewhat less than observed. The wind driven subtropic and subpolar gyre circulations are present, but the western boundary currents are too weak which is a common shortcoming of low-resolution models.

For a faithful representation of changes in the hydrography of the watercolumn and the overturning circulation, a correct simulation of the upper ocean mixed layer and deep water formation processes is essential. Due to the simplicity of the model there are some caveats with respect to this. First, the use of the physically more realistic isopycnal diffusion scheme rather than the conventional horizontal/vertical mixing scheme (as is employed in ECBilt), results in a greatly reduced convective activity (Danabasoglu et al. 1994). This indicates that the coupling of the surface ocean to the deep ocean is too large under the conventional scheme due to

spurious high-latitude convection (Weaver and Wiebe 1999). However, the simulated value of NADW formation is close to a realistic one. The simplicity of the vertical mixing scheme has a more profound effect on the formation of other water masses, as intermediate water or mode water. Second, the sensitivity of the deep ocean geopotential thickness to salinity anomalies is underestimated. The dependency of density variations on salinity is a function of temperature, with higher variations in density if temperature is low. This dependency is fixed in the equation of state in ECBilt at a value which underestimates the density dependency on salinity at low temperatures. These two caveats suggest an over- and undersensitivity of the thermohaline structure of the deep ocean to surface salinity anomalies, respectively. The present results should therefore be regarded as qualitatively correct, but quantitatively uncertain.

## 2.1 Computation of sea level

In the ocean component of ECBilt, the momentum equations are split in a barotropic and a baroclinic part and are solved independently. This facilitates a separate analysis of sea surface height (SSH) variations due to barotropic processes and due to changes in the hydrography of the water column. Both components need to be computed diagnostically from model output, since the ocean component of ECBilt is a rigid-lid ocean where the sea surface topography is reflected in pressure variations exerted by the lid. Moreover, due to the use of the Boussinesq approximation, the model conserves volume rather than mass (Greatbatch 1994), eliminating any explicit contraction or expansion of the water column.

The unit of geopotential thickness is chosen such that a change in geopotential thickness of  $1 \text{ dyn cm} \equiv 1000 \text{ cm}^2 \text{ s}^{-1}$  corresponds to a change in *geometric* thickness of approximately 1 cm (Levitus 1990). Steric sea level is defined as the geopotential thickness of the entire water column. Steric sea level (or geopotential thickness) is computed relative to a standard ocean having homogeneous temperature and salinity of  $0 \text{ }^\circ\text{C}$  and 35 psu, respectively.

The effects of salinity variations on steric sea level and geopotential thickness are computed in this study by substituting for temperature the standard value of  $0 \text{ }^\circ\text{C}$ . The effect of temperature variations is assessed by substituting for salinity the standard value 35 psu.

A detailed explanation of the computation of the steric sea level and the sea level due to barotropic processes can be found in the Appendix.

## 3 Control run: the role of internal variability

### 3.1 Low-frequency sea level variability

We concentrate in this study on sea level variability during *winter* (December–January–February, DJF, for atmospheric variables, January–February–March, JFM, for oceanic variables). The thermohaline structure of the North Atlantic in winter is expected to react more active to changes in solar activity since ocean–atmosphere buoyancy fluxes are largest in this season (Schmitt et al. 1989).

First it is shown that low-frequency SSH variations are dominated by variations in the hydrography of the water column. This source of SSH variability can be distinguished from the other two sources, variations in wind stress and variations in atmospheric pressure, by its frequency characteristics. The spectra of each of the three contributions are computed for each gridbox in the

North Atlantic and then averaged over the North Atlantic. The averaged spectra show that sea level variations due to windstress variations or due to variations in atmospheric pressure display a white spectrum, with energy fairly evenly distributed over the frequency range, while steric sea level variations have a red spectrum, with energy concentrated at the low frequencies. This also holds for spectra averaged over smaller regions in the North Atlantic, like the Gulf Stream region (Fig. 1). Variability of the thermohaline structure of the water column and of the barotropic circulation, and thus of their respective effects on SSH, is expected to be the largest in this region, being the most energetic region in the North Atlantic. It also has our special interest since it borders the US east coast from which the reconstructions of sea level based on foraminiferal proxy records are obtained which have set the framework of this study. Variations in steric sea level become more energetic than variations in sea level due to barotropic processes for periods longer than 10–20 years. Variations in steric sea level dominates sea level pressure variations for periods longer than 4–5 years.

The peak at  $\sim 0.12 \text{ cycles year}^{-1}$  in the steric sea level spectrum is related to baroclinic Rossby waves travelling westwards into the Gulf Stream region.

The spectra (Fig. 1) substantiate that variations in SSH are dominated by variations in steric sea level provided that variability with time scales of 20 years and longer are considered. This is at the high frequency end of the range which can be resolved in the proxy records for sea level, given their sampling resolution of 50–150 years.

### 3.2 Spatial coherency

The standard deviation of winter steric sea level in the North Atlantic is shown in Fig. 2. A local maximum in variability is found just off the US east coast, increasing

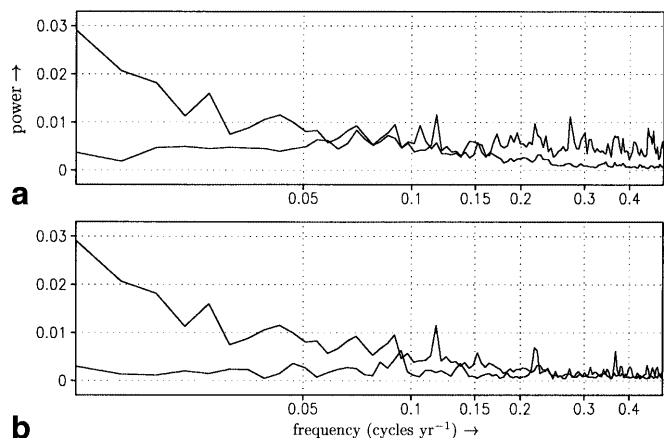


**Fig. 1.** The power spectrum of steric sea level and sea level **a** related to barotropic processes and **b** steric sea level and the inverted barometer effect for the Gulf Stream region ( $14.1^\circ\text{N}$ – $36.6^\circ\text{N}/84.4^\circ\text{W}$ – $56.3^\circ\text{W}$ )

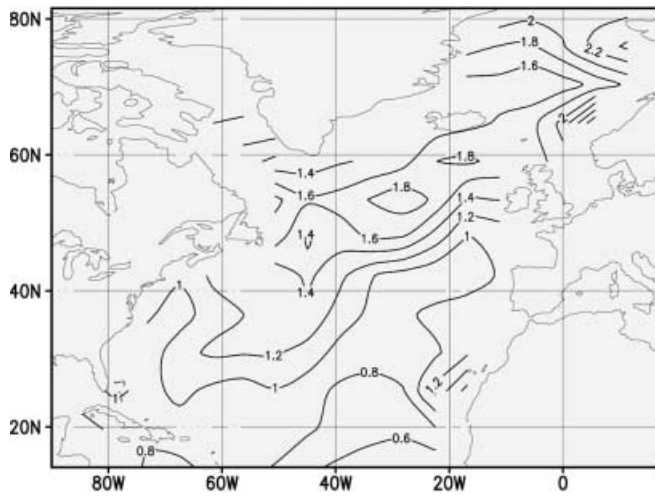


**Fig. 2.** Standard deviation of winter steric sea level in the North Atlantic. Units are dynamic centimetres (dyn cm)

into the northern North Atlantic where the largest amplitude in variability is found. This maximum roughly coincides with the axis of the Gulf Stream and North Atlantic Drift. The observed difference in geopotential height for the 0–1500 m depth interval for the pentads 1955–1959 and 1970–1974 shows similar maxima south of the Gulf Stream reaching 10–17.5 dyn cm (Levitus 1990). The simulated standard deviation of steric sea level in the Gulf Stream region is thus too low. This may be related to the model's coarse resolution, unabling it to faithfully represent steep gradients in sea level. Moreover, the high diffusion (characteristic for low-resolution models) severely damps variability in temperature and salinity at all time scales.

Steric sea level at different points in the North Atlantic which oscillate in concert indicate the presence of some organizing dynamical feature in the ocean. This motivates us to explore steric sea level coherency. Steric sea level just off the eastern coast of North America strongly correlates (at lag zero) with other grid boxes along the eastern North American coast (Fig. 3a). The coherency is oriented along the path of the Gulf Stream and must be related to it. Anomalies in steric sea level can be identified which are advected northwards with the Gulf Stream where the strong circulation elongates them along the US east coast. Thereafter, the sea level anomaly decelerates and reduces in spatial extent.

The correlation (at lag zero) between a grid box in the subtropical gyre and all other North Atlantic grid boxes is high in the vicinity of this grid box, but does not extend into the western boundary region, nor the northern North Atlantic (Fig. 3b). The orientation of this subtropical high coherency region is roughly east–west, suggesting advection of anomalous steric sea level with (baroclinic) Rossby waves since zonal velocities in the subtropical gyre are weak. A similar high coherency is found in steric sea level in the northern North Atlantic (Fig. 3c), which does not extend to more southerly latitudes. This region of high spatial coherency coincides

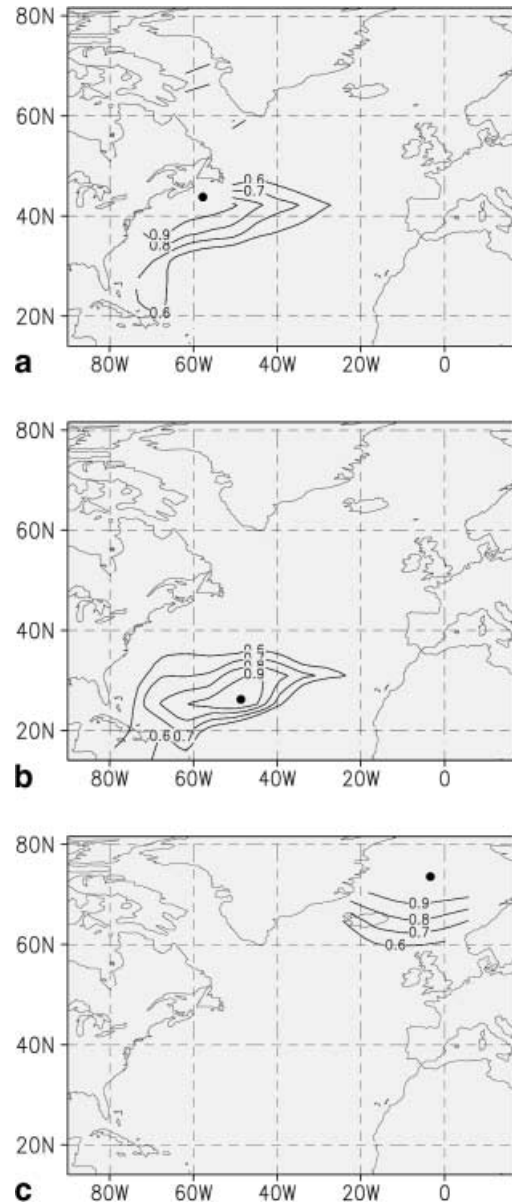


**Fig. 3.** Coherency at lag 0 between **a** a grid box near the US east coast, **b** a grid box in the central subtropics, **c** a grid box in the northern North Atlantic (indicated by the *solid circles*) and all other grid boxes in the North Atlantic. Contours indicating correlations of 0.6 and higher are drawn. The data is low-pass filtered (20 years)

with the area with largest vertical velocities. Deep water is formed here and the hydrography of this region is closely connected to the overturning circulation.

We find that variability in steric sea level in the North Atlantic is characterized by regions of high spatial coherency. High coherencies in steric sea level in these regions validate a spatial averaging over these regions.

### 3.3 Sources of variability of SSH

In the following we will only consider spatially averaged and low-pass filtered (at 40 years) steric sea level

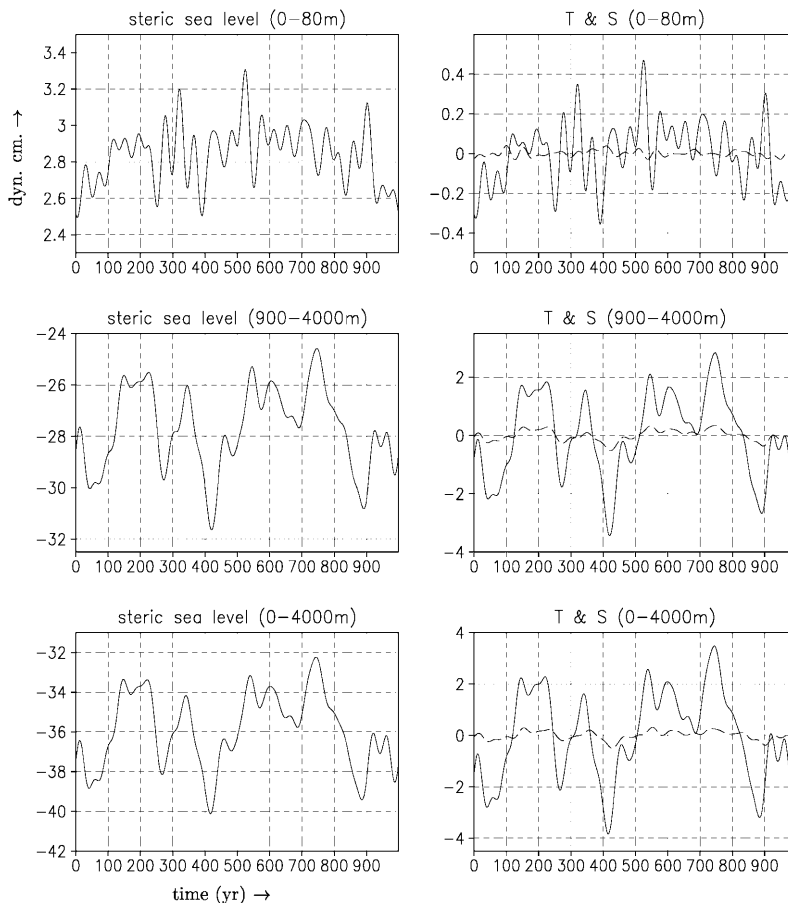
variations. Northern North Atlantic steric sea level is dominated by the contribution of the deep ocean (Fig. 4), which is almost exclusively determined by salinity variations. The geopotential thickness of the two upper layers combined (0–80 m) and the depth interval 80–900 m (not shown) is much smaller than the deep ocean contribution, while the variations in the upper part of the ocean are much more rapid (although the signal has been low-pass filtered at 40 years). The contribution of temperature variations to northern North Atlantic geopotential thickness variability is insignificant in any depth interval. The distinction between the ocean upper and deep layer is inspired by the separation between the northward and southward flowing branches of the overturning and is located between 700 and 1000 m depth. The northern North Atlantic steric sea level is strongly related to overturning (correlation coefficient –0.80, low-pass filtered 40 year) where overturning leads sea level by 12 years. The reason for this high correlation is that variability in the geopotential thickness of the deep ocean (900–4000 m) is dominated by salinity variations in the deep ocean which correlate very well with overturning strength (correlation coefficient 0.84, low-pass filtered 40 years).

Once a salinity anomaly is formed in the deep ocean of the northern North Atlantic, it remains isolated from atmospheric disturbances, and is only subject to diffu-

sion, a parametrization of mixing with other water masses, some zonal spreading and advection along the path of the Deep Western Boundary Current (DWBC) by the overturning circulation. The salinity anomaly is simply advected southward and can still be recognized in the Gulf Stream area steric sea level albeit somewhat ‘smoothed’, diminished in amplitude and with a lag of some 100 years. The Gulf Stream area steric sea level is determined mainly by the same salinity variations in the deep ocean which also dominated steric sea level in the northern North Atlantic. The relative contribution to steric sea level of the upper layers of the ocean is larger in the Gulf Stream compared to that in the northern North Atlantic, and upper layer temperature variations contribute as much to steric sea level as salinity variations.

For the central subtropical North Atlantic similar observations can be made as for Gulf Stream region. A difference between these regions is that the time it takes for the deep-ocean salinity anomaly to spread over the North Atlantic bottom and arrive in the central subtropics is larger compared to that in the Gulf Stream region. The reason is related to the relatively large transports of the DWBC and the slow spreading in zonal direction. Due to the absence of bottom topography in the model, the zonal spreading will be overestimated.

**Fig. 4.** Low-pass filtered (40 year) northern North Atlantic steric sea level and the geopotential thickness of the ocean’s upper layers and the deep ocean. The contributions of salinity and temperature variations are depicted in the *right column* (solid and dashed respectively). Note the change in vertical scale



### 3.4 The dynamical mechanism

We now describe the chain of events that couple variations in the overturning to steric sea level variations. Variations in the overturning are related to variations in the salinity and temperature structure of the North Atlantic and this relation is explored by correlation analysis. All time series were first detrended prior to the correlation analysis. Correlation coefficients are computed over the 1000 year records. The dominant EOF mode of the thermohaline circulation (THC) explains nearly all the low-frequency variability; it is a modulation of the mean overturning. The principal component of this mode is correlated for several lags with the deep ocean (900–4000 m) density due to salinity only ( $\rho_{\text{deep}}^S$ ), with surface density due to salinity changes only ( $\rho_{\text{surf}}^S$ ), with surface density due to temperature changes only ( $\rho_{\text{surf}}^T$ ) and with density due to surface temperature and salinity changes combined ( $\rho_{\text{surf}}$ ) (Fig. 5). These different quantities are averaged horizontally over the sinking region in the North Atlantic, located north of 75°N, before being correlated with overturning strength. Figure 5 shows  $\rho_{\text{surf}}^S$  to lead overturning with 6–9 years, correlating at 0.56. Positive correlation between overturning and salinity extends to the subsurface layers at depth 30–80 m and 80–160 m, but decreases in magnitude. This indicates that salinity anomalies in the upper layers of the ocean induce the fluctuations in the THC. Maximum correlation between  $\rho_{\text{deep}}^S$  and overturning is found at 10–12 years (correlation 0.84), overturning leading deep ocean salinity changes. A negative correlation between  $\rho_{\text{surf}}^T$  and overturning is found, temperature slightly leading. However, temperature does not play a significant role in this process. As SST anomalies

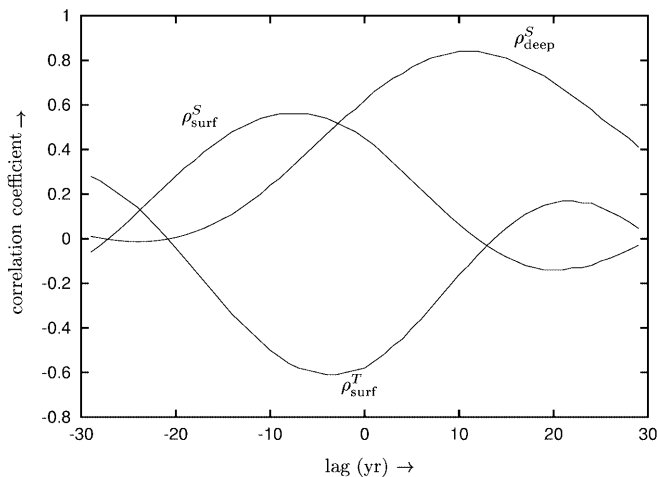


**Fig. 5.** Correlation at various lags for the strength of the thermohaline circulation with deep ocean (900–4000 m) density due to salinity only (short dashed, labelled ' $\rho_{\text{deep}}^S$ '), with surface density due to salinity (long dashed, labelled ' $\rho_{\text{surf}}^S$ ') and surface density due to temperature (solid, labelled ' $\rho_{\text{surf}}^T$ '). All quantities relate to the sinking region in the North Atlantic. Negative lags indicate that overturning lags, positive lags indicate a leading overturning

are much smaller than SSS anomalies, their impact on the density is negligible;  $\rho_{\text{surf}}^S$  is almost equal to  $\rho_{\text{surf}}$ .

The importance of surface salinity anomalies leading overturning and deep ocean salinity anomalies lagging overturning is highlighted in Fig. 6. Correlation coefficients between zonally averaged salinity and overturning are shown at lag  $\pm 10$  years, clearly showing the advection of salinity anomalies by the overturning circulation. Figure 6a shows the correlation at lag  $-10$  years for the upper 700 m of part of the North Atlantic basin. A region with large positive correlation coefficients is found near the surface in the northern North Atlantic. This region of high correlation is observed to move northwards to the sinking region as the lag increases to 0. A similar correlation picture for surface temperature anomalies and overturning shows much more confined regions with lower correlations (Fig. 6b). In Fig. 6c correlation coefficients are shown for lag  $+10$  years, which features large correlation coefficients in the deep ocean. This corresponds to a salinity anomaly penetrating deeply into the sinking region, reaching the bottom. This region of high correlation in the deep ocean is observed to travel southward as lag increases.

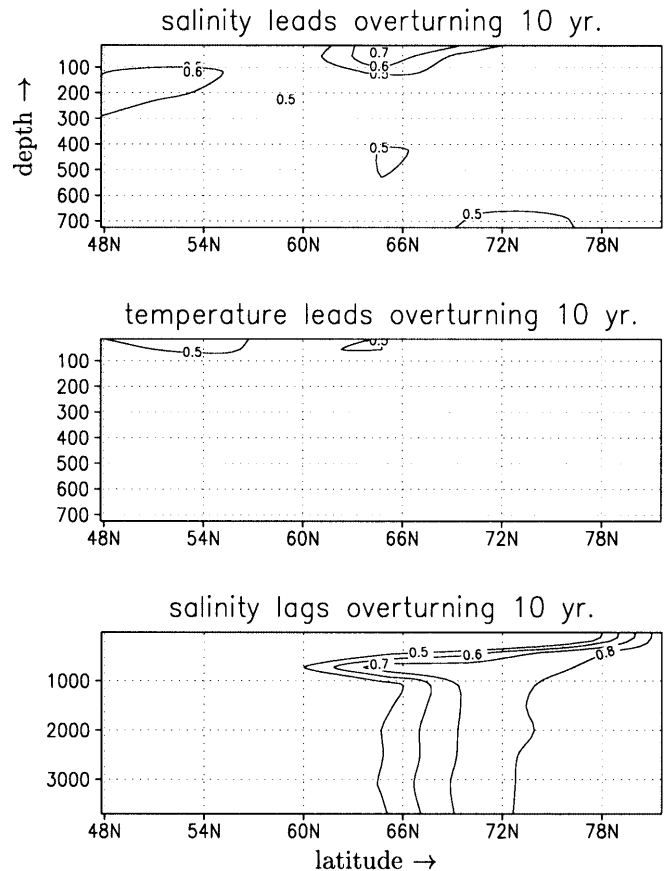


**Fig. 6a–c.** Correlation between zonally averaged salinity and temperature with overturning strength. In **a** salinity leads overturning by 10 year and **b** temperature leads overturning by 10 year (only upper layer of the ocean is shown). In **c** salinity lags overturning by 10 year

The separation depth between the southward and northward moving branches of the THC moves upward in high latitudes. The standard deviation of North Atlantic averaged (north of 59°N) deep ocean salinity is 0.006 psu, the difference between maximum and minimum values reached in the 1000 year simulation is 0.030 psu. For temperature these values are: 0.03 °C and 0.16 °C. The source of salinity anomalies in the northern North Atlantic is advection through the southern boundary of this region, the northern North Atlantic averaged ocean–atmosphere salt flux is a minor contributor. The surface salinity anomalies themselves originate by internal dynamics of the ocean–atmosphere system.

Concluding, in this constant forcing simulation we find that surface salinity anomalies in the northern North Atlantic determine overturning variations. Surface temperature variations are found to be of little importance to overturning variations. Subsequently, the surface salinity anomalies are advected to the deep ocean and this changes the geopotential thickness of the deep ocean. In the northern North Atlantic the deep ocean geopotential thickness dominates steric sea level to a very large degree. The salinity anomaly, and thus the geopotential thickness anomaly, is advected southward with the overturning circulation. Although the amplitude of the salinity anomaly weakens due to mixing with other water masses and zonal spreading, it is found that variations in the geopotential thickness of the deep ocean dominate variations in North Atlantic steric sea level.

## 4 Solar forced run: the pacing of sea level changes

### 4.1 Solar activity

Several hypothesis exist how solar activity influences climate. One of these involves changes of the total solar irradiance (the solar constant) leading to changes in the planetary radiation budget (Lean and Rind 1998). This hypothesis is widely used as a basis for assessing the impact of solar activity on climate in model studies (Crowley 2000; Cubasch et al. 1997; Drijfhout et al. 1999; Haarsma et al. 1999; Rind et al. 1999) and will be used here too.

An alternative hypothesis is that solar activity affect stratospheric ozone through variations in the UV-part of the solar spectrum, which radiatively cool or warm the low and middle stratosphere. This may have consequences for the phase of the North Atlantic Oscillation (NAO). For the ocean, this means that not only heat loss in the subpolar and subtropical gyre change, but also the strength of the wind over the subpolar and subtropical gyres change (Häkkinen 1999; Visbeck et al. 1998). This latter effect will have consequences for sea level change due to windstress variations and will affect the thermohaline structure of the ocean. However, this mechanism will not be considered in the following.

A number of reconstructions for total historic solar irradiance exist which feature similar fluctuations but differ substantially in amplitude. Estimates of a drop in total solar irradiance during the severest part of the Maunder Minimum (1645–1715 AD) range from 0.24% (Lean et al. 1995) and 0.35% (Hoyt and Schatten 1993) to 0.65% (Reid 1997). Here we will use the Reid (1997) time series for total solar irradiance which features this latter scaling factor and extend this to 960 AD by splicing in a proxy record for solar activity based on ice-core measurements of  $^{10}\text{Be}$  and  $^{14}\text{C}$  (Bard et al. 2000) (Fig. 7). This yields a 1000 year long record of approximate irradiance changes. The reason for using the rather large Reid (1997) scaling factor is that the sensitivity to solar irradiance changes in ECBilt is typically a factor 2 too low (Drijfhout et al. 1999), justifying large variations in this parameter.

Considering the simplicity of the model and the uncertainties associated with the solar variability–climate relation, the quantitative aspects of this work should be treated with care. In this study we will concentrate on mechanisms relating sea level to solar forcing and other climate parameters, rather than producing accurate quantitative estimates of historic sea level changes.

### 4.2 Oceanic variability: thermal and haline effects

The trend in the deep ocean temperature and salinity (which have the same values as in the control run) are removed prior to the statistical analysis.

The principal source for low-frequency behaviour of North Atlantic SSH in the solar forced experiment is determined in the same way as in the control run. Spectra of the three sources of SSH variability (variations in the hydrography of the water column, variations

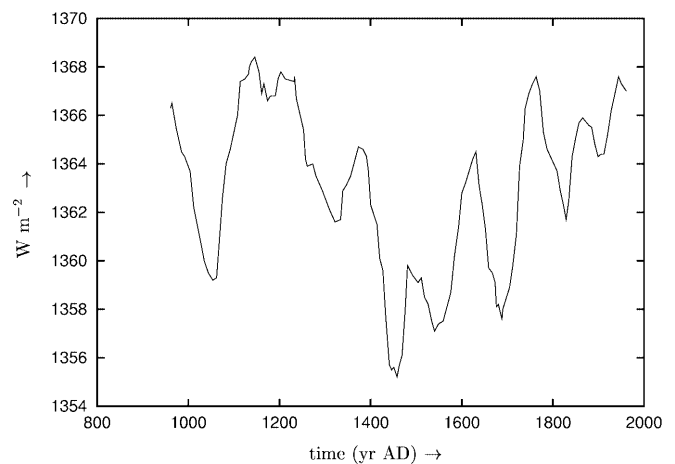


**Fig. 7.** Variations of irradiance based on the cosmogenic isotope record of Bard et al. (2000) combined with the scaling of Reid (1997). A period with high irradiance estimates coincides to a period generally referred to as the Medieval Warm Period (900–1400 AD) and a period with low irradiance estimates coinciding with the Little Ice Age (1500–1750 AD)

in windstress and variations in atmospheric pressure) are computed for each gridbox and then averaged over the complete North Atlantic or the Gulf Stream region. The averaged spectra of steric sea level in the solar forced run is red, but compared to the control run, more energy is concentrated at the lowest frequencies. Although the averaged spectra of sea level due to windstress changes has slightly gained power at low frequencies, it remains white. The relevance of the 'inverted barometer effect' to low frequency SSH variability is negligible, analogous to the control run. Concluding, in the solar forced experiment the dominant source of SSH variations in the North Atlantic is steric sea level, provided that variations with periods longer than 10–20 years are considered.

To further substantiate the relation between steric sea level and solar activity in the model, the averaged steric sea level spectra of the northern North Atlantic (north of 59°N) and that of the Gulf Stream region are computed and correlated with the spectrum of the solar forcing. The correlation coefficient for the northern North Atlantic is 0.72, while for the Gulf Stream region it is somewhat lower at 0.56.

Analogous to the control run, steric sea level is characterized by regions of high spatial coherency (Fig. 8), with the difference that now the spatial extent of these regions is somewhat larger. This indicates that in these regions the strongest sea level response to solar variability is *indirect*, rather than being characterized by a direct, passive thermal expansion response.

Northern Hemisphere averaged surface air temperature (SAT) closely follows the irradiance changes, as is to be expected (not shown).

Analogous to the control run, steric sea level in the northern North Atlantic is mainly determined by salinity variations in the deep ocean (Fig. 9). The variability of the geopotential thickness of the upper oceanic layers is much smaller than the deep ocean contribution. In contrast to the control run, steric sea level contribution of the upper and deep layers feature similar fluctuations on large time scales. Internal variability in surface salinity remains present and can be identified with the small amplitude, high-frequency variations in the upper layer which are absent in the deep ocean. Temperature variations hardly play a role in geopotential thickness at any depth interval. Variations in the deep ocean salinity correlate very well with overturning strength, with overturning leading salinity (maximum correlation 0.88, low-pass filter 40 year, at lag 9–12 years). The deep ocean salinity anomalies are advected southward with the overturning circulation and they arrive, smoothed due to diffusion, some 100 years later in the Gulf Stream region (Fig. 10). The dominant influence of the deep ocean salinity anomaly on steric sea level remains evident. Variations in steric sea level in the solar forced run are roughly a factor two larger than those in the control run and thus closer to observations. The standard deviation of North Atlantic averaged (north of 59°N) deep ocean salinity is 0.010 psu, the difference between max-

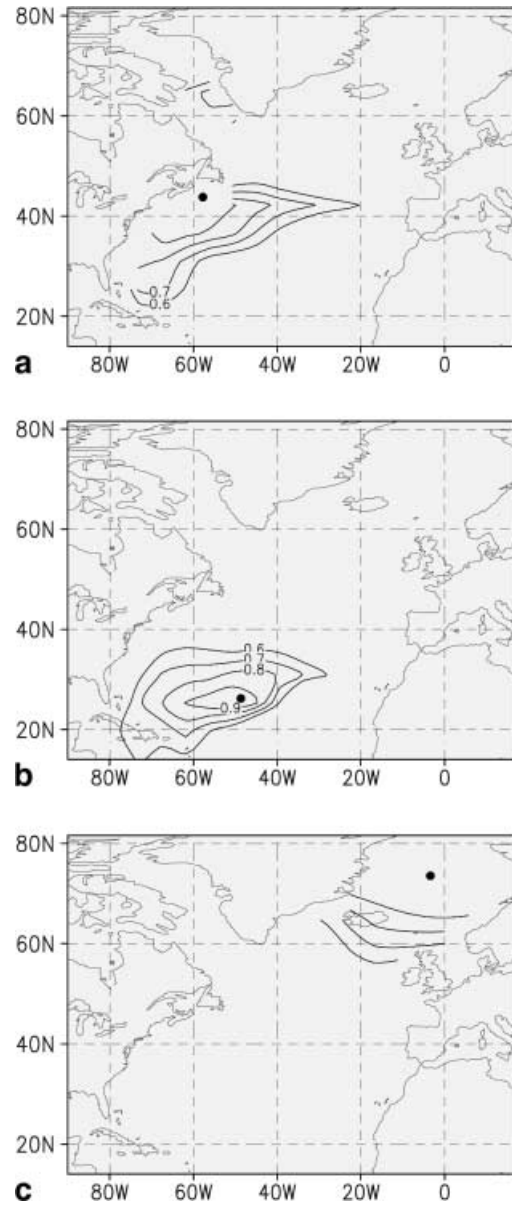
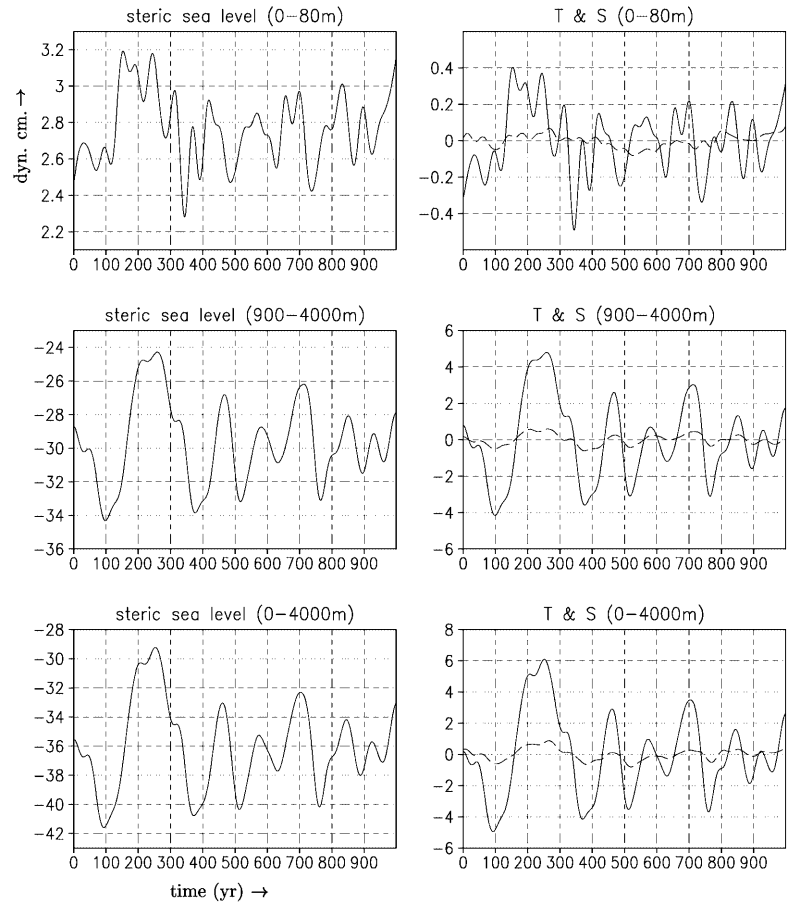


Fig. 8a–c. Same as Fig. 3, but now for the solar forced simulation

imum and minimum values reached in the 1000 year simulation is 0.050 psu. For temperature these values are: 0.05 °C and 0.21 °C.

The high correlation between the spectra of solar forcing and northern North Atlantic averaged steric sea level and that of the Gulf Stream area steric sea level is a reflection of the process described above. In the northern North Atlantic, steric sea level is dominated by the geopotential thickness of the deep ocean (which reflects solar activity) and the uncorrelated noise in the upper layers is small. In the Gulf Stream area the amplitude of the deep ocean geopotential thickness is reduced (although it still dominates steric sea level), and the uncorrelated noise of the upper layers is larger. This makes the impact of noise from upper layers relatively larger.

**Fig. 9.** Same as Fig. 4, but now for the solar forced simulation



#### 4.3 The relation between changes in irradiance and overturning

The generation of a deep ocean salinity anomaly in the solar forced run differs in some aspects from that of the control run. The differences relate directly to the source of the overturning variations; internal dynamics in the control run and external forcing in the solar forced run. The overturning in the latter case is paced by changes in northern North Atlantic surface layer temperature, which directly responds to irradiance changes. Correlation between surface layer temperature and irradiance is 0.7 in the northern North Atlantic.

Higher (lower) surface temperatures in the northern North Atlantic suppress (stimulate) deep-water formation and decrease (increase) the strength of the overturning circulation. In Fig. 11, a correlation analysis between overturning strength and subsurface density changes due to temperature changes only ( $\rho_{\text{surf}}^T$ ), and due to salinity changes only ( $\rho_{\text{surf}}^S$ ), deep ocean density changes due to salinity changes only ( $\rho_{\text{deep}}^S$ ) is shown. These quantities are averaged horizontally over the northern North Atlantic sinking region. Subsurface temperatures and salinities (80–160 m) are used rather than surface quantities since they are less prone to contamination by atmospheric ‘noise’ (using surface quantities reduces the correlation coefficients somewhat). In the control run the reverse seems to be the

case, which reflects the different mechanisms leading to overturning variations: in the control run this atmospheric ‘noise’ in the surface layer triggers deep water formation.

In the solar forced simulation  $\rho_{\text{surf}}^T$  is *positively* correlated to overturning, maximally correlating when *leading* with 8–14 years (coefficient: 0.49). The source of the surface temperature anomalies is obviously the changing solar irradiance. Overturning and irradiance strongly anti-correlate at  $-0.79$ , where overturning lags irradiance with 12–19 years. With a lag of 4–7 years,  $\rho_{\text{surf}}^S$  maximally correlates at 0.84 with overturning. A sluggish (fierce) overturning transports less (more) high salinity water northwards from the subtropics and, moreover, it exposes surface waters longer (shorter) to precipitation in the northern North Atlantic. The anomalously low (high) surface salinity water is advected with the overturning, producing, some time later, a deep ocean negative (positive) salinity anomaly. At lag 9–12 years,  $\rho_{\text{deep}}^S$  maximally correlates (0.88) with overturning. It is interesting that  $\rho_{\text{surf}}^T$  correlates less well with overturning variations than irradiance:  $\rho_{\text{surf}}^T$  modulate the overturning slightly which leads to sea surface salinity anomalies that enforce the effect of irradiance on the overturning.

The variations in overturning due to the variations in solar activity can be strong. In particular the decrease in irradiance between the Medieval Warm Period and the

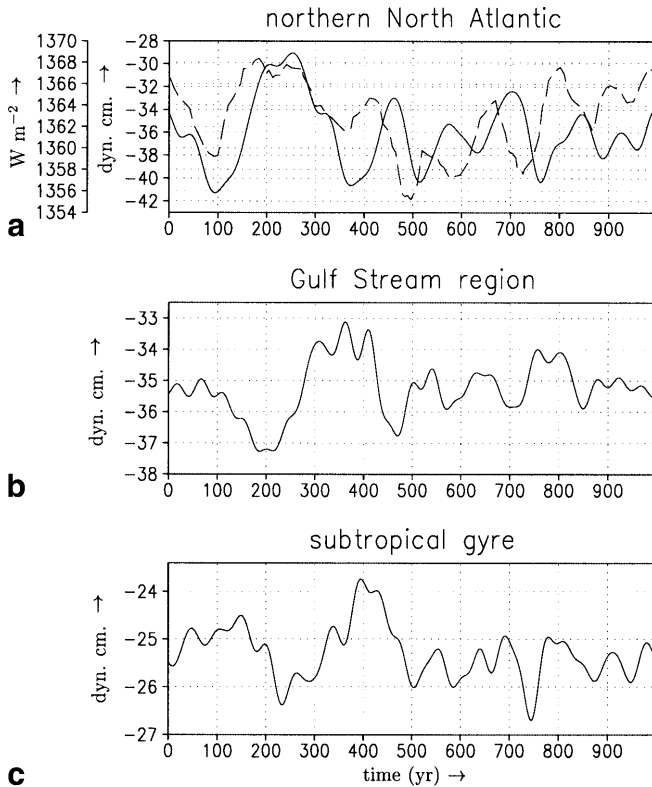


**Fig. 10.** Irradiance variations (*dashed*) and steric sea level (*solid*) in **a** the northern North Atlantic, **b** in the Gulf Stream region and **c** in the subtropical gyre. Anomalies in sea level can be seen to move southward. The anomalies decrease in magnitude with decreasing latitude. The influence of relatively high-frequency, low-amplitude steric sea-level variations, which can be related to upper layer dynamics, is evident in **b** and **c**. Note the change in *vertical scale*

Little Ice Age was accompanied by a strong increase in overturning strength. The difference in the 50-year averages in volume transport between the 1150–1200 and 1425–1475 intervals (see Fig. 7) amounts to over 15% (2.1 Sv).

Again surface layer salinity anomalies play an important role in generating the overturning variations, but now they are not exclusively generated by internal dynamics, but by surface temperature (irradiance) forced overturning variations.

A similar strong anti-correlation between irradiance and the strength of the overturning has also been found in the ECHAM3/LSG ocean–atmosphere coupled model (Cubasch et al. 1997), with overturning lagging irradiance.

## 5 Discussion and conclusions

The model results indicate that variability of steric sea level in the North Atlantic is mainly determined by variations in the geopotential thickness of the deep ocean (900–4000 m), which result almost exclusively from variations in deep ocean salinity. Temperature variations at any depth do not contribute significantly to

variations in steric sea level in the North Atlantic. This holds for both the control and the solar forced simulation.

Pattullo et al. (1955) report that on the seasonal time scale in low and temperate regions steric sea level is associated mainly with temperature fluctuations in the upper 100 m. The results presented here indicate that on decadal–centennial time scales the opposite is true, i.e. steric sea level is determined mainly by deep ocean salinity fluctuations. On the seasonal time scale, the ocean–atmosphere thermal buoyancy flux exhibit large variations which dominate changes in the thermohaline structure of the entire water column. On the other hand, the characteristic time scale of the deep ocean is orders of magnitude larger than the seasonal time scale and is comparable to the length of the tide gauge records on which Pattullo et al. (1955) based their observation.

The source of the northern North Atlantic deep ocean salinity anomalies in the control simulation is related to the variability of the overturning circulation and to surface salinity anomalies that are generated by internal dynamics of the ocean–atmosphere system. The surface salinity anomalies stimulate or suppress overturning, which advects these anomalies to the deep ocean. This mechanism is to a high degree similar to the one proposed by Delworth et al. (1993) which led in their model to a self-sustained oscillation with a period broadly centred at 50 years.

In the solar forced simulation, the source of the northern North Atlantic deep ocean salinity anomalies is a modulation of the overturning. Overturning variations are paced by northern North Atlantic surface temperatures which stimulate or suppress overturning. Surface temperatures passively follow irradiance fluctuations. A slow down (speed up) of the overturning advects less (more) high salinity waters from the subtropics to the northern North Atlantic and surface waters remain a longer (shorter) period in a region with net precipitation. This makes the surface waters less (more) salty than on average. The salinity anomaly generated in this way is advected with the overturning circulation to the deep ocean and is subsequently advected southwards with the Deep Western Boundary Current.

In the constant forcing simulation, steric sea level changes are forced by salinity anomalies in the northern North Atlantic rather than by temperature anomalies, as is the case in the solar forced experiment. Since SAT and SST are closely coupled on long time scales (Drijfhout et al. 2001), a relation between sea level and (European) climate is found in the solar forced simulation. However, a relation between steric sea level and (European) climate is absent in the control simulation, since the former only relates well to surface salinity anomalies rather than surface temperature anomalies. Surface temperature anomalies may be induced by changes in the overturning, but the spatial extent of any effects will be drowned in the climatic noise; they will only influence the regional climate (given that the changes in overturning circulation are relatively small).

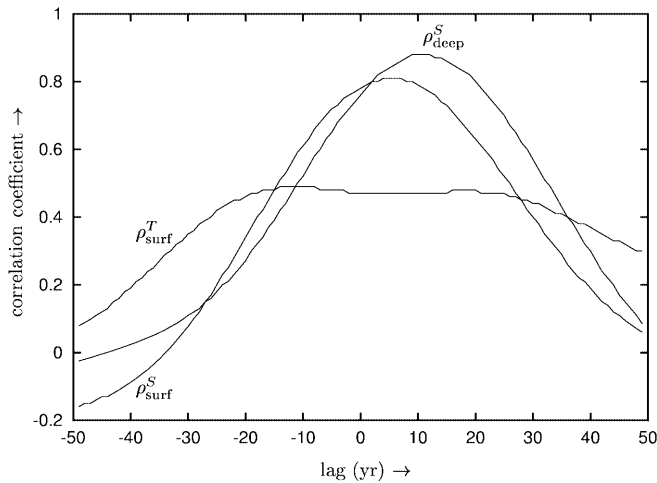


Fig. 11. Same as Fig.5, but now for the solar forced simulation

A similar forced experiment has been conducted using a solar irradiance estimate based on the same cosmogenic isotope record, but spliced to the Lean et al. (1995) scaling factor which is 2–3 times smaller than that of Reid (1997); giving similar fluctuations but substantially different amplitudes. Northern North Atlantic steric sea level in the solar forced simulation using the Lean et al. (1995) scaling factor (in short: the Lean simulation) differed from that in the solar forced simulation using the larger Reid (1997) scaling factor (in short: the Reid simulation) with respect to the amplitude and the timing of the sea level fluctuations. Steric sea level in the northern North Atlantic in both simulations follow (with a lag) the decrease in irradiance around 1000 AD (Fig. 7), the increase to the Medieval Warm Period and then the sharp decrease in the year 1320 AD. Sea level variations in the Lean simulation associated with this change in irradiance are about 10 dyn cm, while variations in the Reid simulation reach more than 13 dyn cm. Steric sea level variations in both simulations then reach maxima at model year 450 (1410 AD), but then the pacing of the northern North Atlantic sea level fluctuations in the simulations start to diverge. This is particularly clear in the strength of the overturning. Overturning in the Reid simulation keeps close track with the irradiance variations; for the period 500–1000 (model) years, the correlation is  $-0.71$ , lagging irradiance with 9–13 yr, while the correlation in the Lean simulation over the period 500–1000 (model) years varies between  $-0.28$  and  $-0.33$  at this lag. The low correlation is a reflection of the dominance of internal variability in the Lean simulation. The presently identified process clearly depends on the amplitude of the forcing and sensitivity of the atmosphere-ocean system to this forcing.

The validity of the simulations critically depends on the representation of processes in the ocean mixed layer and of deep water formation processes. However, the relation between anomalies in the hydrography and

overturning seem robust. It is not likely to be dependent on details of the vertical mixing. This is confirmed by the Cubasch et al. (1997) simulations, where a state-of-the-art ocean model is used, giving qualitatively the same relation between North Atlantic hydrography and overturning.

This study provides a framework to interpret the recent proxy based reconstructions for low-frequency sea-level variations in the North Atlantic. Existing explanations for observed variability in proxy records for sea level at the US coast include abrupt and repeated changes in the wind driven surface circulation of the North Atlantic (Fletcher et al. 1993) and steric sea level rise due to temperature variations in the upper layer (Fletcher et al. 1993; Gehrels 1999; van de Plassche et al. 1998). Although these proposed mechanisms have implications for sea level change on seasonal to interannual time scales (Greatbatch et al. 1996; Pattullo et al. 1955), the results presented here suggest that geopotential thickness variations of the deep ocean dominate low-frequency (decadal–centennial) behaviour. Furthermore, the results indicate that the main response in steric sea level to irradiance changes is an indirect one, involving variations in the thermohaline circulation rather than being directly related to a cooling or warming of the oceanic upper layers.

**Acknowledgements** We would like to thank Dr. O. van de Plassche (Vrije Universiteit Amsterdam) for his interest, Drs. F. M. Selten and R. J. Haarsma (KNMI) for their continued support and two anonymous reviewers for their constructive suggestions. This research was sponsored by the Dutch National Research Programme (NRP) on Global Air Pollution and Climate Change; registered under 951268, entitled: ‘Ocean-climate variability and sea level in the North Atlantic region since AD 0’.

## Appendix A

### Computation of sea level in ECBilt

#### A.1 Sea level related to barotropic processes

The barotropic dynamics in the ocean is computed by constructing an equation for the barotropic stream function. This is simplified by replacing the Laplacian friction by linear friction for reasons related to the coarseness of the grid (Haarsma et al. 1996), and the inertia term is neglected. This results in the simple Stommel equation for wind driven barotropic flow (Haarsma et al. 1996). In this equation, the pressure gradient terms are lost, but these terms represent the effects of the sea surface height on the barotropic circulation and need to be recovered. We start with the (vertically averaged) equations of motion:

$$-f\bar{\mathbf{v}} = \frac{-1}{\rho_0 H} \int_{-H}^0 \frac{\partial p}{\partial x} - \kappa_s \bar{\mathbf{u}} + \frac{\kappa}{H} \frac{\partial \bar{\mathbf{u}}}{\partial z} \Big|_{-H}^0 \quad (\text{A1a})$$

$$f\bar{\mathbf{u}} = \frac{-1}{\rho_0 H} \int_{-H}^0 \frac{\partial p}{\partial y} - \kappa_s \bar{\mathbf{v}} + \frac{\kappa}{H} \frac{\partial \bar{\mathbf{v}}}{\partial z} \Big|_{-H}^0 \quad (\text{A1b})$$

Here  $\bar{\mathbf{u}}$  is the barotropic velocity,  $f$  the Coriolis parameter,  $H$  the depth of the ocean,  $\rho_0$  a standard value of sea water density,  $p$  is the pressure exerted by the rigid lid and  $\kappa_s$  is the linear friction coef-

ficient. The wind stress ( $\tau_x$ ,  $\tau_y$ ) enters the equations through the terms

$$\frac{\partial u}{\partial z} \Big|_0 = \frac{\tau_x}{\rho_0} \quad (\text{A2a})$$

$$\frac{\partial v}{\partial z} \Big|_0 = \frac{\tau_y}{\rho_0} . \quad (\text{A2b})$$

Given the velocity field  $\mathbf{u}$ , it is possible to compute the gradients of the vertically averaged pressure,

$$\frac{\partial \bar{p}}{\partial x} = \frac{1}{H} \int_{-H}^0 \frac{\partial p}{\partial x} \quad \text{and} \quad \frac{\partial \bar{p}}{\partial y} = \frac{1}{H} \int_{-H}^0 \frac{\partial p}{\partial y} , \quad (\text{A3})$$

since all terms in the equation (A1) are known except these pressure terms. The pressure  $p$  is written as

$$p(x, y, z) = p_s(x, y) + p^*(x, y, z) , \quad (\text{A4})$$

where  $p_s$  is the surface pressure and  $p^*$  is the hydrostatic contribution:

$$p^*(x, y, z) = \int_z^0 \rho(x, y, z') g \, dz' . \quad (\text{A5})$$

At each grid point an equation can be formulated with which the pressure has to comply with. This is done by taking the divergence (rather than the curl) of (A1):

$$\left( \frac{\partial^2}{\partial x^2} + \frac{\partial^2}{\partial y^2} \right) \bar{p} = \rho_0 H f \left( \frac{\partial \bar{v}}{\partial x} - \frac{\partial \bar{u}}{\partial y} \right) + \frac{\partial \tau_x}{\partial x} + \frac{\partial \tau_y}{\partial y} . \quad (\text{A6})$$

The problem to be solved is:

$$\nabla^2 \bar{p} = f(x, y) \quad (\text{A7a})$$

$$\frac{\partial \bar{p}}{\partial n} \Big|_{\text{boundary}} = g(x, y) . \quad (\text{A7b})$$

The Poisson equation (A7) is discretized on the grid. This yields a system of algebraic equations of five-point molecule form,

$$\mathbf{M} \cdot \mathbf{t} = \mathbf{q} \quad (\text{A8})$$

where at each grid point the formula

$$a_{ij} t_{i,j-1} + b_{ij} t_{i-1,j} + c_{ij} t_{ij} + d_{ij} t_{i+1,j} + e_{ij} t_{i,j+1} = q_{ij} \quad (\text{A9})$$

must be formulated (Kreyszig 1993). The matrix equation (A8) is solved directly using NAG's F04ATF routine. Surface pressure is computed by subtracting the hydrostatic contribution (A5). The solution to equation (A7) is not unique due to the Neumann boundary conditions (any constant can be added) and at each time step the spatial average of the surface pressure field is set to zero. The excess pressure is then converted into height of the water column (with density  $1025 \text{ kg m}^{-3}$ ) using the hydrostatic approximation.

## A.2 Sea level related to hydrography; steric sea level

The geopotential thickness,  $\Delta D$ , between two constant pressure surfaces,  $p_1$  and  $p_2$ , in the ocean is defined as (Levitus 1990; Neumann and Pierson 1966):

$$\Delta D = \int_{p_1}^{p_2} [\alpha(S, T, p) - \alpha(35\text{‰}, 0^\circ\text{C}, p)] dp \quad (\text{A10})$$

in which  $\alpha(S, T, p)$  represents specific volume (in  $\text{cm}^3 \text{ g}^{-1}$ ) at salinity  $S$  (per mil), temperature  $T$  ( $^\circ\text{C}$ ) and pressure  $p$  (decibars). The quantity  $\alpha(35\text{‰}, 0^\circ\text{C}, p)$  represents the specific volume of a 'standard' ocean.

In the calculations however, geopotential thickness between surfaces of constant depth is computed. Pressure in units of decibars was replaced by depth in units of centimeters. The pressure differential  $dp$  was replaced by  $\bar{\rho} g dz$ , in which  $\bar{\rho}$  represents a constant density of magnitude 1.02 in units of grams per cubic centimeter,  $g$  had a value of  $980 \text{ cm s}^{-2}$ , and  $dz$  represents the difference in centimeters between two surfaces of constant depth for simplicity of calculation (the approximation is good enough if large-scale distribution of differences in the vertical are considered, Levitus 1990).

The units of geopotential thickness are those of specific energy  $1000 \text{ cm}^2 \text{ s}^{-2}$  (dynamic centimeters). These units are chosen so that a change in specific energy of  $1000 \text{ cm}^2 \text{ s}^{-2}$  (1 dyn cm) corresponds to a change in geometric thickness of approximately 1 cm.

Following Levitus (Levitus 1990) we refer to geopotential thickness  $\Delta D$  as the steric sea level (Pattullo et al. 1955) if the upper range of integral (A10) is the sea surface. In this case the lower surface will be considered an equipotential surface.

## References

- Bard E, Raisbeck G, Yiou F, Jouzel J (2000) Solar irradiance during the last 1200 years based on cosmogenic nuclides. *Tellus* 52B: 985–992
- Barnett TP (1989) A solar-ocean relation: fact or fiction? *Geophys Res Lett* 16: 803–806
- Crowley TJ (2000) Causes of climate change over the past 1000 years. *Science* 289: 270–277
- Crowley TJ, Kim K-Y (1999) Modeling the temperature response to forced climate change over the last six centuries. *Geophys Res Lett* 26: 1901–1904
- Cubasch U, Voss R, Hegerl GC, Waszkewitz J, Crowley TJ (1997) Simulation of the influence of solar radiation variations on the global climate with an ocean-atmosphere circulation model. *Clim Dyn* 13: 757–767
- Danabasoglu G, McWilliams JC, Gent PR (1994) The role of mesoscale tracer transports in the global ocean circulation. *Science* 264: 1123–1126
- Delworth T, Manabe S, Stouffer RJ (1993) Interdecadal variations of the thermohaline circulation in a coupled ocean-atmosphere model. *J Clim* 6: 1993–2011
- Drijfhout SS, Haarsma RJ, Opsteegh TD, Selten FM (1999) Solar-induced versus internal variability in a coupled climate model. *Geophys Res Lett* 26: 205–208
- Drijfhout SS, Kattenberg A, Haarsma RJ, Selten FM (2001) The role of the ocean in midlatitude, interannual to decadal time scale climate variability of a coupled model. *J Clim* 14: 3617–3630
- Ezer T (2001) Can long-term variability in the Gulf Stream transport be inferred from sea level? *Geophys Res Lett* 28: 1031–1034
- Fletcher CH, Van Pelt JE, Brush GS, Sherman J (1993) Tidal wetland record of Holocene sea-level movements and climate history. *Palaeogeograph Palaeoclim Palaeoecol* 102: 177–213
- Gehrels WR (1999) Middle and Late Holocene sea-level changes in eastern Maine reconstructed from foraminiferal saltmarsh stratigraphy and AMS  $^{14}\text{C}$  dates on basal peat. *Quat Res* 52: 350–359
- Goosse H, Selten FM, Haarsma RJ, Opsteegh JD (2000) Decadal variability in high northern latitudes as simulated by an intermediate complexity climate model. *Ann Glacio* 33: 1–21
- Greatbatch RJ (1994) A note on the representation of steric sea level in models that conserve volume rather than mass. *J Geophys Res (Oceans)* 99: 12,767–12,771
- Greatbatch RJ, Fanning AF, Goulding AD (1991) A diagnosis of interpentadal circulation changes in the North Atlantic. *J Geophys Res (Oceans)* 96: 22,009–22,023
- Greatbatch RJ, Lu Y, de Young B (1996) Application of a barotropic model to North Atlantic synoptic sea level variability. *J Mar Res* 54: 451–469

- Haarsma RJ, Selten FM, Opsteegh JD, Lenderink G, Liu Q (1996) ECBILT: a coupled atmosphere ocean sea-ice model for climate predictability studies. Tech Rep, KNMI
- Haarsma RJ, Drijfhout SS, Opsteegh JD, Selten FM (2000) The impact of solar forcing on the variability in a coupled climate model. *Space Sci Rev* 94: 287–294
- Haarsma RJ, Opsteegh JD, Selten FM, Wang X (2001) Rapid transitions and ultra-low frequency behaviour in a 40 kyr integration with a coupled climate model of intermediate complexity. *Clim Dyn* 17: 559–570
- Haih JD (1996) The impact of solar variability on climate. *Science* 272: 981–984
- Häkkinen S (1999) Variability of the simulated meridional heat transport in the North Atlantic for the period 1951–1993. *J Geophys Res (Oceans)* 104: 10,991–11,007
- Häkkinen S (2001) Variability in sea surface height: a qualitative measure for the meridional overturning in the North Atlantic. *J Geophys Res (Oceans)* 106: 13,837–13,848
- Hoyt DV, Schatten KH (1993) A discussion of plausible solar irradiance variations, 1700–1992. *J Geophys Res (Atmospheres)* 98: 18,895–18,906
- Kreyszig E (1993) *Advanced engineering mathematics*. John Wiley and Sons, New York
- Lean J, Rind D (1998) Climate forcing by changing solar radiation. *J Clim* 11: 3069–3094
- Lean J, Beer J, Bradley R (1995) Reconstruction of solar irradiance since 1610: implications for climate change. *Geophys Res Lett* 22: 3195–3198
- Levitus S (1990) Interpentadal variability of steric sea level and geopotential thickness on the North Atlantic Ocean, 1970–1974 versus 1955–1959. *J Geophys Res (Oceans)* 95: 5233–5238
- Neumann G, Pierson WJ (1966) *Principles of physical oceanography*. Prentice-Hall, Englewood Cliffs, N.J., USA
- Opsteegh JD, Haarsma RJ, Selten FM, Kattenberg A (1998) ECBILT, a dynamic alternative to mixed boundary conditions in ocean models. *Tellus* 50A: 348–367
- Pattullo J, Munk W, Revelle R, Strong E (1955) The seasonal oscillation in sea level. *J Mar Res* 14: 88–113
- Reid GC (1997) Solar forcing of global climate change since the mid-17th century. *Clim Change* 37: 391–405
- Reid GC (1999) Solar variability and its implications for the human environment. *J Atmos Solar-Terr Phys* 61: 3–14
- Renssen H, Goosse H, Fichefet T, Campin J-M (2001) The 8.2 kyr BP event simulated by a global atmosphere–sea-ice–ocean model. *Geophys Res Lett* 28: 1567–1570
- Rind D, Lean J, Healey R (1999) Simulated time-dependent climate response to solar radiative forcing since 1600. *J Geophys Res (Atmospheres)* 104: 1973–1990
- Schmitt RW, Bogden PS, Dorman CE (1989) Evaporation minus precipitation and density fluxes for the North Atlantic. *J Phys Ocean* 19: 1208–1221
- Selten FM, Haarsma RJ, Opsteegh JD (1999) On the mechanism of North Atlantic decadal variability. *J Clim* 12: 1956–1973
- van de Plassche O. (2000) North Atlantic climate–ocean variations and sea-level in Long Island Sound, Connecticut, since 500 cal yr AD. *Quat Res* 53: 89–97
- van de Plassche O, van der Borg K, de Jong AFM (1998) Sea level–climate correlation during the past 1400 years. *Geology* 26: 319–322
- van der Schrier G, Versteegh GJM (2001) Internally and externally forced climate variability: a dynamical systems approach using the Central England temperature record. *Geophys Res Lett* 28: 759–762
- van Loon H, Labitzke K (1998) The global range of the stratospheric decadal wave. Part I: its association with the sunspot cycle in summer and in the annual mean, and with the troposphere. *J Clim* 11: 1529–1537
- van Loon H, Labitzke K (1999) The signal of the 11-year solar cycle in the global stratosphere. *J Atmos Solar-Terr Phys* 61: 53–61
- Visbeck M, Cullen H, Krahnemann G, Naik N (1998) An ocean model’s response to North Atlantic Oscillation-like wind forcing. *Geophys Res Lett* 25: 4521–4524
- Weaver AJ, Wiebe EC (1999) On the sensitivity of projected oceanic thermal expansion to the parametrisation of sub-grid scale ocean mixing. *Geophys Res Lett* 26: 3461–3464
- Weber SL (2001) The impact of orbital forcing on the climate of an intermediate-complexity coupled model. *Global Planet Change* 30: 7–12
- White WB, Lean J, Cayan DR, Dettinger MD (1997) Response of global upper temperature to changing solar irradiance. *J Geophys Res (Oceans)* 102: 3255–3266